025921-9-T

AN ASYMPTOTIC ANALYSIS OF THE PLANE WAVE SCATTERING BY A SMOOTH CONVEX IMPEDANCE CYLINDER

Hasnain H. Syed and John L. Volakis
Department of Electrical Engineering
and Computer Science
The University of Michigan
Ann Arbor, MI 48109-2122

January 1990

Northrop Corp.
8900 E. Washington Blvd.
Pico Rivera, CA 90660

An Asymptotic Analysis of the Plane Wave Scattering by a Smooth Convex Impedance Cylinder

Hasnain H. Syed and John L. Volakis
Radiation Laboratory
Department of Electrical Engineering and Computer Science
The University of Michigan
Ann Arbor, MI 48109-2122

Abstract

A rigorous UTD (Uniform Geometrical Theory of Diffraction) analysis of the diffraction by a smooth convex impedance cylinder is presented. The analysis parallels the one employed for the perfectly conducting cylinder. Ray solutions are obtained which remain valid in the transition region and uniformly reduce to those in the lit and the shadow regions. In addition, a ray solution is presented when the observation point is in the close vicinity of the cylinder. The resulting transition region expressions are in terms of Fock-type integrals which are evaluated using a numerical scheme based on Fourier quadrature.

I. Introduction

The problem of scattering by a smooth convex impedance cylinder has received much attention. Wang [1, 2] presented ray-optical solutions for the impedance and coated cylinders. His results are valid only in the lit and shadow regions and do not apply to the case where the observation point is in the close vicinity of the cylinder. Wait and Conda [3, 4] developed a solution which is valid in the transition region and for observation points on and off the surface. However, as pointed out by Pathak [5] it did not uniformly reduce to the ray solution [6, 7] exterior to the transition regions. Also, it is not valid on the surface in the transition region and these limitations were the primary motivation of Pathak's work [5] for the perfectly conducting convex cylinder. Recently, Kim and Wang [13] presented a solution applicable to a coated circular cylinder that remained valid in the transition region fields. They employed a heuristic approach to obtain the numerical values of the resulting transition integral applicable to a coated cylinder. Their solution is uniform but not applicable to the close vicinity of the cylinder.

In this report we present a rigorous UTD solution of the diffraction by a circular impedance cylinder with plane wave illumination. The analysis parallels Pathak's formulation [5] for the perfectly conducting cylinder. Using this procedure, ray solutions are obtained that are valid in the transition region and reduce uniformly to those in the lit and shadow regions. In addition, a ray solution is given when the observation point is in the close vicinity of the cylinder as shown by the regions 4, 5, and 6 in fig. 1. Finally, the presented UTD solution is generalized to the case of a smooth convex cylinder in a heuristic fashion paralleling the approach followed for the perfectly conducting case.

II. Mathematical Formulation

Before considering the problem of surface wave diffraction by a convex impedance surface, it is instructive to first develop a solution for the diffraction by the canonical geometry of a circular impedance cylinder. Generalizations to any convex surface can then be made on the basis of the expressions obtained for the circular cylinder.

Consider the circular impedance cylinder, shown in fig. 2, illuminated by a z-polarized plane wave field given by

$$u^i = u_o\, e^{jkx} = u_o\, e^{jk\rho\cos\phi} \tag{1}$$

where u_o denotes the amplitude (possibly complex) of the wave and an $e^{j\omega t}$ time dependence is assumed and suppressed. The total field in the presence of the impedance cylinder can be easily written in terms of the eigenfunction representation

$$u^{total} = \sum_{n=-\infty}^{\infty} j^n \left[J_n(k\rho) + A_n\, H_n^{(2)}(k\rho) \right] e^{-jn\phi} \tag{2}$$

where

$$A_n = -\frac{J_n'(ka) + QJ_n(ka)}{H_n^{(2)\prime}(ka) + QH_n^{(2)}(ka)} \tag{3}$$

$$Q = \begin{cases} -j\eta & \text{for } H_z\text{-incidence} \\ -j\dfrac{1}{\eta} & \text{for } E_z\text{-incidence} \end{cases} \tag{4}$$

η is the normalized surface impedance of the cylinder, a is the cylinder radius and ϕ ($\phi = \phi_s$ at the shadow boundary) is the angle measured from the x-axis. Furthermore, the indicated differentiations of the Bessel and Hankel functions are with respect to the argument.

Since (2) is a slowly convergent series, especially for large ka, our objective is to obtain asymptotic representations for u^{total} suitable for practical applications. We, therefore, seek uniform expressions for the total field in the lit, shadow and transition regions. Such expressions should also recover the well known geometrical optics field, where applicable.

By rewriting (2) in an integral form and subsequently employing the Watson's transformation, we find that [8]

$$u^{total} = u_1 + u_2 = u_o \int_{-\infty}^{\infty} \left[J_\upsilon(k\rho) - \frac{J_\upsilon'(ka) + QJ_\upsilon(ka)}{H_\upsilon^{(2)\prime}(ka) + QH_\upsilon^{(2)}(ka)} H_\upsilon^{(2)}(k\rho) \right]$$

$$\bullet\, e^{-j\upsilon\psi}\, d\upsilon + u_2 \tag{5}$$

where

$$u_2 = u_o \int_{-\infty}^{\infty} \left[J_\upsilon(k\rho) - \frac{J_\upsilon'(ka) + QJ_\upsilon(ka)}{H_\upsilon^{(2)\prime}(ka) + QH_\upsilon^{(2)}(ka)} H_\upsilon^{(2)}(k\rho) \right] e^{+j\upsilon\frac{\pi}{2}}$$

$$\bullet\, \frac{e^{-j\upsilon(2\pi + \phi)} + e^{-j\upsilon(2\pi - \phi)}}{1 - e^{-j2\upsilon\pi}}\, d\upsilon \tag{6}$$

$$\psi = |\phi| - \frac{\pi}{2} \qquad |\phi| < \pi \;\text{ or }\; |\psi| < \frac{\pi}{2} \tag{7}$$

and u_2 denotes the creeping waves which circulate around the cylinder more than once. We will consider this term later in the analysis.

An alternate expression for u_1 is

$$u_1 = \frac{u_o}{2} \int_{-\infty}^{\infty} \left[H_\upsilon^{(1)}(k\rho) - \frac{H_\upsilon^{(1)\prime}(ka) + QH_\upsilon^{(1)}(ka)}{H_\upsilon^{(2)\prime}(ka) + QH_\upsilon^{(2)}(ka)} H_\upsilon^{(2)}(k\rho) \right] e^{-j\upsilon\psi}\, d\upsilon \tag{8}$$

and when this is combined with the expression of u_1 in (5), we find that

$$u_1 = I_1 + I_2 \tag{9}$$

where

$$I_1 = mu_o \int_{c_1+c_2} J_\upsilon(k\rho)\, e^{-j\upsilon(\tau)\psi}\, d\tau - \frac{mu_o}{2} \int_{c_1} H_\upsilon^{(2)}(k\rho)\, e^{-j\upsilon(\tau)\psi}\, d\tau \tag{10}$$

$$I_2 = -mu_o \int_{c_2} \frac{J_\upsilon'(ka) + QJ_\upsilon(ka)}{H_\upsilon^{(2)\prime}(ka) + QH_\upsilon^{(2)}(ka)}\, H_\upsilon^{(2)}(k\rho)\, e^{-j\upsilon(\tau)\psi}\, d\tau$$

$$-\frac{mu_o}{2} \int_{c_1} \frac{H_\upsilon^{(1)\prime}(ka) + QH_\upsilon^{(1)}(ka)}{H_\upsilon^{(2)\prime}(ka) + QH_\upsilon^{(2)}(ka)}\, H_\upsilon^{(2)}(k\rho)\, e^{-j\upsilon(\tau)\psi}\, d\tau \tag{11}$$

and

$$\upsilon(\tau) = ka + m\tau \ ; \qquad m = \left(\frac{ka}{2}\right)^{\frac{1}{3}} \tag{12}$$

In addition, the contour c_1 runs from $-\infty - j\varepsilon$ to $0 - j\varepsilon$ and the contour c_2 runs from $0 - j\varepsilon$ to $\infty - j\varepsilon$, where $\varepsilon \to 0^+$. The use of $H_\upsilon^{(1)}(k\rho) = 2J_\upsilon(k\rho) - H_\upsilon^{(2)}(k\rho)$ has also been involved to obtain the above expression.

From (10), we observe that I_1 is independent of the impedance boundary conditions, whereas I_2 is completely dependent on the form of the boundary conditions. We next approximate the Bessel function $J_\upsilon(ka)$ and the Hankel function $H_\upsilon^{(1),(2)}(ka)$ in (11) for large ka by

$$J_\upsilon(ka) \approx (m\sqrt{\pi})^{-1}\, V(\tau) \tag{13a}$$

$$H_\upsilon^{(1),(2)}(ka) \approx \mp j\, (m\sqrt{\pi})^{-1}\, W_{1,2}(\tau) \tag{13b}$$

where the Airy function $V(\tau)$ and $W_{1,2}(\tau)$ are defined as [9]

$$2j\, V(\tau) = W_1(\tau) - W_2(\tau) \tag{13c}$$

$$W_{1,2}(\tau) = \frac{1}{\sqrt{\pi}} \int_{\Gamma_{1,2}} e^{\tau t - t^3/3}\, dt \tag{13d}$$

The contour Γ_1 runs from $\infty e^{-j\frac{2\pi}{3}}$ to $\infty - j\varepsilon$ and Γ_2 is the complex conjugate of Γ_1.

Using (13), I_2 can now be written as

$$I_2 = jmu_o \int_{c_2} \frac{V'(\tau) - qV(\tau)}{W_2'(\tau) - qW_2(\tau)} H_\upsilon^{(2)}(k\rho)\, e^{-j\upsilon(\tau)\psi}\, d\tau$$

$$+ \frac{mu_o}{2} \int_{c_1} \frac{W_1'(\tau) - qW_1(\tau)}{W_2'(\tau) - qW_2(\tau)} H_\upsilon^{(2)}(k\rho)\, e^{-j\upsilon(\tau)\psi}\, d\tau \tag{14}$$

where

$$q = \begin{cases} -j\left(\frac{ka}{2}\right)^{\frac{1}{3}} \eta & \text{for } H_z\text{-incidence} \\ -j\left(\frac{ka}{2}\right)^{\frac{1}{3}} \eta & \text{for } E_z\text{-incidence} \end{cases} \tag{15}$$

(a) Analysis for the shadowed portion of the transition region

The uniform asymptotic evaluation of I_1 for large $k\rho$ is known for the shadow part of the transition region [5] and is given by

$$I_1 \approx \frac{e^{-j\frac{\pi}{4}}}{\sqrt{2\pi k}} \frac{e^{-jka\theta}}{\theta} F\left(\frac{ks\theta^2}{2}\right) \frac{e^{-jks}}{\sqrt{s}} \tag{16}$$

where all parameters are defined in fig. 3 and

$$F(x) = 2j\sqrt{x}\; e^{jx} \int_{x}^{\infty} e^{-jx^2}\, dx \tag{17}$$

is a modified Fresnel integral referred to as the transition function [10]. Also, positive branch of $\sqrt{ks\theta^2/2}$ is chosen in (16).

For the evaluation of I_2 in (14), we must employ the Debye approximation for $H_{\upsilon}^{(2)}(k\rho)$ [8] given by

$$H_{\upsilon}^{(2)}(k\rho) \sim \sqrt{\frac{2}{\pi k\rho \sin\gamma}}\; \exp\left(-jk\rho \sin\gamma + j\upsilon\gamma + j\frac{\pi}{4}\right) \tag{18}$$

$$\upsilon = k\rho\cos\gamma \qquad\qquad 0 < \mathrm{Re}\,\gamma < \pi$$

Since $\upsilon(\tau) = ka + m\tau$ is of order ka in the transition region, we may also set $\sin\gamma \approx \frac{s}{\rho}$ in the Debye approximation to obtain

$$H_{\upsilon(\tau)}^{(2)}(k\rho) \sim \sqrt{\frac{2}{\pi ks}}\; e^{-jks + j\frac{\pi}{4}}\; e^{j(ka + m\tau)\beta_s} \tag{19}$$

An evaluation of I_2 then yields

$$I_2 \sim -u_o \frac{e^{-j\frac{\pi}{4}}}{\sqrt{2\pi k}} \frac{e^{-jka\theta}}{\theta} \frac{e^{-jks}}{\sqrt{s}} - u_o m \sqrt{\frac{2}{k}}\; e^{-jka\theta}\, G(x, q) \frac{e^{-jks}}{\sqrt{s}} \tag{20}$$

where G(x, q) is the generalized Pekeris' function [11] defined by

$$G(x, q) = \frac{e^{-j\frac{\pi}{4}}}{\sqrt{\pi}} \int_{-\infty}^{\infty} \frac{V'(\tau) - qV(\tau)}{W_2'(\tau) - qW_2(\tau)}\, e^{-jx\tau}\, d\tau \tag{21}$$

$$x = m\theta \qquad\qquad (x > 0 \text{ in the shadow region})$$

An evaluation of G(x, q), which is computationally efficient, can be found in [12].

Combining (16) and (20) yields

$$u_1(P_s) \sim -u^i(Q_1)\, m \sqrt{\frac{2}{k}}\, e^{-jka\theta} \left[\frac{e^{-j\frac{\pi}{4}}}{2x\sqrt{\pi}} \left\{ 1 - F\left(\frac{ks\theta^2}{2} \right) \right\} + G(x, q) \right] \frac{e^{-jks}}{\sqrt{s}} \tag{22}$$

where P_s is a point in the shadow region and $u^i(Q_1) = u_o$ is the value of the incident field at Q_1.

In the deep shadow region (far from SB_1), $\theta \gg 0$, $x \gg 0$, $F\left(\frac{ks\theta^2}{2}\right) \to 1$ and the solution in (22) reduces to the GTD solution.

(b) Analysis for the illuminated portion of the transition region

If the result in (22) for the shadow region is directly employed to calculate the field u_1 at a point P_L in the lit region, it does not reduce to the geometrical optics field far from SB_1. An approximation for $H_\upsilon^{(2)}(k\rho)$ which is different from that in (19) is, therefore, required to model the field behavior in the deep lit region. First, $H_{\upsilon(\tau)}^{(2)}(k\rho)$ in I_2 of (14) is replaced by its far zone approximation ($\upsilon(\tau) \ll k\rho$) to obtain

$$I_2 \approx \sqrt{\frac{2}{\pi k\rho}}\, e^{-j\left(k\rho - \frac{\pi}{4}\right)} u_o \left[jm \int_{c_2} \frac{V'(\tau) - qV(\tau)}{W_2'(\tau) - qW_2(\tau)}\, e^{j\upsilon(\tau)\left(\frac{\pi}{2} - \psi\right)} d\tau \right.$$

$$\left. + \frac{m}{2} \int_{c_1} \frac{W_1'(\tau) - qW_1(\tau)}{W_2'(\tau) - qW_2(\tau)}\, e^{j\upsilon(\tau)\left(\frac{\pi}{2} - \psi\right)} d\tau \right] \tag{23}$$

One may next approximate $\upsilon(\tau)\left(\frac{\pi}{2} - \psi\right)$ in the exponent of (23) as [5]

$$\upsilon(\tau)\left(\frac{\pi}{2} - \psi\right) = (ka + m\tau)\, 2\tilde{\gamma} \approx -ka \left\{ \frac{x'}{m} + \frac{1}{24} \frac{(x')^3}{m^3} \right\} - \tau x' \tag{24}$$

where

$$\frac{\pi}{2} - \psi = 2\,\tilde{\gamma}$$

$$x' = -2m \sin \tilde{\gamma}$$

$$-\tilde{\gamma} = \sin^{-1} \frac{x'}{2m} = \left(\frac{1}{2m}\right) x' + \frac{1}{6}\left(\frac{1}{2m}\right)^3 (x')^3 + \frac{3}{40}\left(\frac{1}{2m}\right)^5 (x')^5 + \ldots$$

$$\text{with } \left(\frac{x'}{2m}\right)^2 < 1$$

Using (24) in (23) yields

$$I_2 \sim -u_o \sqrt{\frac{2}{k\rho}}\; e^{-jk\rho} \left[m \exp\left\{ j2ka \sin\tilde{\gamma} - j\,\frac{(x')^3}{12} \right\} \right.$$

$$\left. \cdot \left\{ \frac{e^{-j\frac{\pi}{4}}}{2x'\sqrt{\pi}} + G(x', q) \right\} \right] \tag{25}$$

In the far zone ($k\rho \gg ka$), we have (see fig. 4)

$$\phi \approx 2\theta^i \tag{26a}$$

$$\frac{e^{-jk\rho}}{\sqrt{\rho}} \approx \frac{e^{-jk(\ell + a\cos\theta^i)}}{\sqrt{\ell}} \tag{26b}$$

and

$$\sin\tilde{\gamma} = \sin\left(\frac{\pi - |\phi|}{2}\right) \approx \sin\left(\frac{\pi - 2\theta^i}{2}\right) \tag{26c}$$

Therefore, I_2 can be written as

$$I_2 \sim -u_o \sqrt{\frac{2}{k\ell}}\, e^{-jk(\ell + a\cos\theta^i)}\, m \exp\left\{ j2ka\cos\theta^i - j\frac{(x')^3}{12} \right\}$$

$$\cdot \left\{ \frac{e^{-j\frac{\pi}{4}}}{2x'\sqrt{\pi}} + G(x', q) \right\} \tag{27}$$

with

$$x' = -2m\cos\theta^i \tag{28}$$

Using the approximation in (24) and (26), I_1 is evaluated to find [5]

$$I_1 \sim u^i(P_L) + u_o m \frac{e^{-j\frac{\pi}{4}}}{\sqrt{2\pi k}\; x'} \exp\left\{ j2ka\cos\theta^i - j\frac{(x')^3}{12} \right\}$$

$$\cdot F(2k\ell\cos^2\theta^i)\, \frac{e^{-jk(\ell + a\cos\theta^i)}}{\sqrt{\ell}} \qquad (k\rho \gg ka) \tag{29}$$

Combining (27) and (29) we further obtain

$$u_1(P_L) \sim u^i(P_L) + u^i(Q_R)\left[-m\sqrt{\frac{2}{k}} \exp\left\{ -j\frac{(x')^3}{12} \right\} \right.$$

$$\left. \cdot \left\{ \frac{e^{-j\frac{\pi}{4}}}{2x'\sqrt{\pi}} \left[1 - F(2k\ell\cos^2\theta^i)\right] + G(x', q) \right\} \right] \frac{e^{-jk\ell}}{\sqrt{\ell}} \tag{30}$$

where

$$u^i(Q_R) = u_o\, e^{jka\cos\theta^i}$$

Also, by virtue of the identification

$$\frac{a\cos\theta^i}{2} = \tilde{\rho} = \text{reflected ray caustic distance} \tag{31}$$

in (30), we can rewrite $u_1(P_L)$ as

$$u_1(P_L) \sim u^i(P_L) + u^i(Q_R)\left[-\sqrt{\frac{-4}{x'}}\ \exp\left\{-j\frac{(x')^3}{12}\right\}\right.$$

$$\left.\cdot\left\{\frac{e^{-j\frac{\pi}{4}}}{2x'\sqrt{\pi}}\left[1 - F(2k\ell\cos^2\theta^i)\right] + G(x', q)\right\}\right]\sqrt{\frac{\bar{\rho}}{\ell}}\ e^{-jk\ell} \tag{32}$$

The near-zone (not in the close vicinity of the surface) field in the lit region can now be obtained from (32) by replacing the far-zone ray divergence factor $\sqrt{\bar{\rho}/\ell}$ with its near-zone value $\sqrt{\bar{\rho}/(\bar{\rho}+\ell)}$, where ℓ represents the near-zone reflected ray distance from Q_R to P_L.

Therefore,

$$u_1(P_L) \sim u^i(P_L) + u^i(Q_R)\left[-\sqrt{\frac{-4}{x'}}\ \exp\left\{-j\frac{(x')^3}{12}\right\}\right.$$

$$\left.\cdot\left\{\frac{e^{-j\frac{\pi}{4}}}{2x'\sqrt{\pi}}\left[1 - F(2k\ell\cos^2\theta^i)\right] + G(x', q)\right\}\right]\sqrt{\frac{\bar{\rho}}{\bar{\rho}+\ell}}\ e^{-jk\ell} \tag{33}$$

The above result, which is valid within the lit region (including the shadow boundary SB_1) now properly reduces to the GTD solution in the deep lit region. It remains to evaluate the contribution of u_2. This can be expressed as a residue series but is negligible in the lit region for large ka.

III. Generalization to the Case of a Smooth Convex Cylinder

By utilizing the local properties of propagation, scattering, and diffraction of waves at high frequencies, the uniform results in (22) and (33) can be modified to the case of a convex cylinder of slowly varying curvature in the following manner

(a) Shadow region

The field u_1 at P_s in (22) after generalization becomes

$$u_1(P_s) \sim -u^i(Q_1)\sqrt{m(Q_1)\,m(Q_2)}\;\sqrt{\frac{2}{k}}\;e^{-jkt}\left[\frac{e^{-j\frac{\pi}{4}}}{2x\sqrt{\pi}}\right.$$

$$\left.\cdot\left\{1 - F(kL\tilde{a})\right\} + G(x, q)\right]\frac{e^{-jks}}{\sqrt{s}} \qquad x \geq 0 \tag{34}$$

where

$$x = \int_{Q_1}^{Q_2} \frac{m(t')}{\rho_g(t')}\,dt' \tag{35a}$$

$$t = \int_{Q_1}^{Q_2} dt' \tag{35b}$$

$$m(t') = \left[\frac{k\rho_g(t')}{2}\right]^{\frac{1}{3}} \tag{35c}$$

$$L = S \tag{35d}$$

$$\tilde{a} = \frac{x^2}{2m(Q_1)\,m(Q_2)} \tag{35e}$$

t' denotes any point between Q_1 and Q_2 on the cylinder and $\rho_g(t')$ is the radius at t'.

(b) Lit region

The field u_1 at P_L in the lit zone of the convex cylinder, after generalizing (33), becomes

$$u_1(P_L) \sim u^i(P_L) + u^i(Q_R)\left[-\sqrt{\frac{-4}{x'}}\exp\left\{\frac{-j(x')^3}{12}\right\}\left\{\frac{e^{-j\frac{\pi}{4}}}{2x'\sqrt{\pi}}\right.\right.$$

$$\left.\left.\bullet\left(1 - F\left[kL'\,\tilde{a}'\right]\right) + G(x', q)\right\}\right]\sqrt{\frac{\tilde{\rho}}{\tilde{\rho} + \ell}}\; e^{-jk\ell} \qquad x' \le 0 \tag{36}$$

where

$$x' = -2m\,(Q_R)\cos\theta^i \tag{37a}$$

$$m(Q_R) = \left[\frac{k\rho_g(Q_R)}{2}\right]^{\frac{1}{3}} \tag{37b}$$

$$\tilde{\rho} = \frac{\rho_g(Q_R)\cos\theta^i}{2} \tag{37c}$$

and

$$L' = \ell \tag{37d}$$

$$\tilde{a} = 2\cos^2\theta^i \tag{37e}$$

IV. Field in the Deep Lit and Shadow Regions

The geometrical optics incident and reflected rays represent an accurate first-order asymptotic high-frequency field approximation within the deep lit region. These fields can be obtained via an asymptotic evaluation of the first term [14] of (5) yielding

$$u_1^{GO}(P_L) \sim u^i(P_L) + u^i(Q_R)\,R_{s,h}\sqrt{\frac{\tilde{\rho}}{\tilde{\rho} + \ell}}\; e^{-jk\ell} \tag{38}$$

in which

$$R_s \approx \frac{\eta \cos \theta^i - 1}{\eta \cos \theta^i + 1} \qquad (E_z \text{ - incidence}) \tag{39a}$$

$$R_h \approx \frac{\cos \theta^i - \eta}{\cos \theta^i + \eta} \qquad (H_z\text{-incidence}) \tag{39b}$$

are the surface reflection coefficients.

For the field in the deep shadow region, a residue series solution can be obtained from the first integral in (5) which gives the creeping-wave representation as

$$u_1 = -u_o \frac{4}{ka} \sum_{n=1}^{\infty} \frac{H_{\upsilon_n}^{(2)}(k\rho)\, e^{-j\upsilon_n\left(\phi - \frac{\pi}{2}\right)}}{H_{\upsilon_n}^{(2)}(ka) \frac{\partial}{\partial \upsilon} \left[H_{\upsilon}^{(2)'}(ka) + QH_{\upsilon}^{(2)}(ka)\right]_{\upsilon = \upsilon_n}} \tag{40}$$

where υ_n are the zeros of the following transcendental equation

$$H_{\upsilon_n}^{(2)'}(ka) + QH_{\upsilon_n}^{(2)}(ka) = 0 \tag{41}$$

The contribution from the multiply encircling wave represented by u_2 in (16) can also be cast into a residue series. We have

$$u_2 = -u_o \frac{4}{ka} \sum_{n=1}^{\infty} \frac{H_{\upsilon_n}^{(2)}(k\rho)\, e^{j\upsilon_n \frac{\pi}{2}}}{H_{\upsilon_n}^{(2)}(ka) \frac{\partial}{\partial \upsilon} \left[H_{\upsilon}^{(2)'}(ka) + QH_{\upsilon}^{(2)}(ka)\right]_{\upsilon = \upsilon_n}}$$

$$\bullet \frac{e^{-j\upsilon_n(2\pi + \phi)} + e^{-j\upsilon_n(2\pi - \phi)}}{1 - e^{-j2\upsilon_n\pi}} \tag{42}$$

Clearly, the above expression for u_2 fails when one of the poles υ_n is equal to an integer and corresponds to a resonance condition.

The residue series given in (40) does not give the ray-picture interpretation of the creeping-wave diffraction. In order to obtain the Keller type GTD ray format, the Debye approximation can be employed for the Hankel function for $k\rho \gg |\upsilon_n|$, i.e.,

$$H^{(2)}_{\upsilon_n}(k\rho) \approx \sqrt{\frac{2}{\pi k\rho \sin\beta_s}}\; e^{-j\left(k\rho \sin\beta_s - \beta_s\upsilon_n - \frac{\pi}{4}\right)} \tag{43}$$

where

$$\beta_s = \cos^{-1}\left(\frac{\upsilon_n}{k\rho}\right) \tag{44}$$

Further, assuming

$$\beta_s \approx \cos^{-1}\left(\frac{a}{\rho}\right), \tag{45}$$

(43) can be rewritten as

$$H^{(2)}_{\upsilon_n}(k\rho) \approx \sqrt{\frac{2}{\pi ks}}\; e^{-j\left[ks - \upsilon_n \cos^{-1}\left(\frac{a}{\rho}\right) - \frac{\pi}{4}\right]} \tag{46}$$

where

$$s = \sqrt{\rho^2 - a^2} \tag{47}$$

Substituting (43) - (47) into (40) now yields

$$u_1^d \approx -u^i(Q_1) \sum_{n=1}^{\infty} \left[\mathfrak{D}_n(Q_1) \cdot e^{-j\upsilon_n\theta} \cdot \mathfrak{D}_n(Q_2)\right] \frac{e^{-jks}}{\sqrt{ks}} \tag{48}$$

where

$$\theta = \psi - \beta_s \tag{49}$$

(see figure 3 for the angle definitions) and for the circular cylinder

$$\mathfrak{D}_n(Q_1) = \mathfrak{D}_n(Q_2) = \left[\sqrt{\frac{2}{\pi}}\ \frac{4}{ka}\ \frac{e^{j\frac{\pi}{4}}}{H_{\upsilon_n}^{(2)}(ka)\ \frac{\partial}{\partial\upsilon}\left[H_\upsilon^{(2)'}(ka) + QH_\upsilon^{(2)}(ka)\right]_{\upsilon = \upsilon_n}} \right]^{1/2} \tag{50}$$

A ray representation for the multiply encirculing wave u_2 can also be obtained in a similar fashion.

V. Field in the Close Vicinity of the Convex Cylinder

The uniform results given in (34) and (36) are not valid in the close neighborhood of the surface of the cylinder. To describe the field in the close vicinity of the surface, a Taylor series approximation of the Fock integrals is required.

When the field point is extremely close to the surface of a circular cylinder such that $k(\rho - a) \gg ka$, $J_{\upsilon(\tau)}(k\rho)$ and $H_{\upsilon(\tau)}^{(1),(2)}(k\rho)$ can be approximated by

$$J_\upsilon(k\rho) \approx (m\sqrt{\pi})^{-1}\ V(\tau - h) \tag{51}$$

$$H_\upsilon^{(1),\,(2)}(k\rho) \approx \mp j(m\sqrt{\pi})^{-1}\ W_{1,2}(\tau - h) \tag{52}$$

where

$$h = m^{-1}\ kd \tag{53a}$$

$$d = \rho - a \tag{53b}$$

Using the above approximations and (13) in the expressions for u_1 given by (5) and (8), we have

$$u_1 \approx \frac{e^{-jka\psi}}{\sqrt{\pi}}\ u_0 \int_{-\infty}^{\infty} \left[V(\tau - h) - \frac{V'(\tau) - qV(\tau)}{W_2'(\tau) - qW_2(\tau)}\ W_2(\tau - h) \right] e^{-jz\tau}\, d\tau \tag{54}$$

and

$$u_1 \approx \frac{-ju_0}{2\sqrt{\pi}} e^{-jka\psi} \int_{-\infty}^{\infty} \left[W_1(\tau - h) - \frac{W_1'(\tau) - qW_1(\tau)}{W_2'(\tau) - qW_2(\tau)} W_2(\tau - h) \right] e^{-jz\tau} d\tau \tag{55}$$

where

$$z = m\psi \tag{56}$$

It is convenient to employ the representation (54) for $\psi < 0$ and that of (55) for $\psi > 0$. Also, we may rewrite (54) in terms of a new parameter z' as used by Logan [11] for the Fock currents (h=0 case). We have

$$z' = m \sin \psi = -m \cos \phi \tag{57}$$

$$\psi = \sin^{-1} \frac{z'}{m} = \frac{z'}{m} + \frac{1}{6} \frac{(z')^3}{m} + \ldots \qquad \text{if} \left(\frac{z'}{m}\right)^2 < 1 \tag{58}$$

Therefore,

$$e^{-jz\tau} \approx e^{-jz'\tau},$$

$$e^{-jka\psi} \approx \exp\left\{ jka \cos \phi - j \frac{(z')^3}{3} \right\}$$

and (54) can then be written as

$$u_1(P)\Big|_{\psi<0} \approx u_o e^{jka \cos \phi} \frac{\exp\left\{-j \frac{(z')^3}{3}\right\}}{\sqrt{\pi}}$$

$$\cdot \int_{-\infty}^{\infty} \left[V(\tau - h) - \frac{V'(\tau) - qV(\tau)}{W_2'(\tau) - qW_2(\tau)} W_2(\tau - h) \right] e^{-jz'\tau} d\tau \tag{59}$$

The result in (55) and (59) can be further generalized to the case of arbitrary convex cylinder as follows:

$$u_1(P) \approx u^i(P_N)\,\frac{\exp\left\{-j(z')^3/3\right\}}{\sqrt{\pi}}$$

$$\cdot \int_{-\infty}^{\infty}\left[V(\tau - h) - \frac{V'(\tau) - qV(\tau)}{W_2'(\tau) - qW_2(\tau)}\, W_2(\tau - h)\right] e^{-jz'\tau}\, d\tau \tag{60a}$$

where $z' = -m(P_N)\cos\theta^i$ for P_N in the lit region and

$$u_1(P) \approx u^i(Q_1)\,\frac{-j\,e^{-jkt}}{2\sqrt{\pi}} \int_{-\infty}^{\infty}\left[W_1(\tau - h) - \frac{W_1'(\tau) - qW_1(\tau)}{W_2'(\tau) - qW_2(\tau)}\, W_2(\tau - h)\right] e^{-jz\tau}\, d\tau \tag{60b}$$

where

$$z = \int_{Q_1}^{P_N} \frac{m(t')}{\rho_g(t')}\, dt' \qquad \text{for } P_N \text{ in the shadow region}$$

$$t = \int_{Q_1}^{P_N} dt'$$

The point P_N in the lit and shadow regions is illustrated in fig. 5.

In order to simplify the integrals in (60a) and (60b), $W_{1,2}(\tau - h)$ may be approximated by a Taylor series for small h as

$$W_{1,2}(\tau - h) = W_{1,2}(\tau) - W_{1,2}'(\tau)h + \tau W_{1,2}(\tau)\frac{h^2}{2} - \left[W_{1,2}(\tau) + \tau W_{1,2}'(\tau)\right]\frac{h^3}{3!}$$

$$+\left[2W_{1,2}'(\tau) + \tau^2 W_{1,2}(\tau)\right]\frac{h^4}{4!} - \left[4\tau W_{1,2}(\tau) + \tau^2 W_{1,2}'(\tau)\right]\frac{h^5}{5!} + 0(h^6). \tag{61}$$

Also

$$\frac{1}{\sqrt{\pi}}\int_{-\infty}^{\infty} V(\tau - h)\, e^{-jz'\tau}\, d\tau = e^{-jhz'}\; e^{j(z')^3/3} \tag{62}$$

Using (61) and (62), in conjunction with (60a) and (60b), we obtain

$$u_1(P) \sim u^i(P_N)\left[e^{-jhz'} - \sum_{n=0}^{5} \frac{(-1)^2}{n!} (jhz')^n + e^{-j(z')^3/3} \left\{\Lambda_h(z') - q\Lambda_s(z')\right\}\right] \tag{63a}$$

for P_N in lit region,

$$u_1(P) \sim u^i(Q_1)\, e^{-jkt} \left[\frac{\rho_g(P_N)}{\rho_g(Q_1)}\right]^{\frac{-1}{6}} \left\{\Lambda_h(z) - q\Lambda_s(z)\right\} \tag{63b}$$

for P_N in shadow region where

$$\Lambda_s(D) = hg(D) + \frac{jh^3}{3!} g'(D) - 2\frac{h^4}{4!} g(D) - \frac{h^5}{5!} g''(D) + 0(h^6) \tag{64a}$$

$$\Lambda_h(D) = g(D) + \frac{jh^2}{2!} g'(D) - \frac{h^3}{3!} g(D) - \frac{h^4}{4!} g''(D) - \frac{j4h^5}{5!} g'(D) + 0(h^6) \tag{64b}$$

$$g(D) = \frac{1}{\sqrt{\pi}} \int_{-\infty}^{\infty} \frac{e^{-jD\tau}}{W_2'(\tau) - qW_2(\tau)}\, d\tau \tag{65}$$

A procedure for the computation of g(D) is discussed by Pearson [12]. It should be noted that (63a) which is applicable in the lit region may not be of sufficient accuracy in the case of slowly attenuating creeping and/or surface waves. An improved result can then be obtained by adding (63a) and (63b) with $t > \pi a$. Clearly, the addition of (63b) corresponds to the contribution of the creeping wave that has travelled the minimum distance on the cylinder's surface to reach P_N. The contribution of those creeping waves that travelled more than once is given by (42) and could be added to u_1 if greater accuracy is required.

VI. Numerical Results

The UTD expressions (22), (33) , (38), (48) and (63) provide a complete set of equations for the computation of the total field in any region of interest. These maintain field continuity at all transition boundaries which is an important feature not shared by alternative expressions found in the literature.

In this section we present some curves which validate the accuracy of the derived expressions by comparison with data based on the eigenfunction solution. A difficulty in implementing these was the evaluation of Fock-type functions G(x, q) and g(D) as well as the determination of the zeros corresponding to (41). The Fock-type functions were evaluated by employing the Fourier quadrative method as described in [12] and the zeros of (41) were determined using the routine given in [15]. Since of primary interest is the evaluation of the field very close to the impedance surfaces, we have concentrated in the presentation of data pertaining to this case. Figures 6-10 present the magnitude of the field 0.05λ away from the surface of circular impedance cylinder of radius 3λ. Each figure corresponds to a different surface impedance and includes data for both polarizations of incidences. As seen, in all cases, the accuracy of the UTD solution is excellent. An exception to this is the case depicted in figure 10 where the chosen impedance yields a pole that is close to an integer. As discussed earlier, this specifies a resonance condition. Nevertheless, the agreement between the UTD and eigenfunction solutions is excellent in the shadow region.

At present we are continuing with the integration of all of the UTD expressions in a single versatile code. This will be followed by a similar analysis based on using higher order impedance boundary conditions.

Acknowledgements

The authors are indebted to Dr. L. Wilson Pearson for providing the subroutines for the computation of the Fock-type functions. The complex zero search routine was provided by Mr. Stanley Locus.

References

[1] N. Wang, "Regge poles, natural frequencies, and surface wave resonance of a circular cylinder with a constant surface impedance," IEEE Trans. Antennas Propagat., Vol. AP-30, Nov. 1982.

[2] -----, "Electromagnetic scattering from a dielectric coated circular cylinder," IEEE Trans. Antennas Propagat., Vol. AP-33, Sept. 1985.

[3] J.R. Wait and A.M. Conda, "Diffraction of electromagnetic waves by smooth obstacles for grazing angles," J. Res. Bur. Stand., Vol. 63D, pp. 181-197, 1959.

[4] -----, "Pattern of an antenna on a curved lossy surface," IRE Trans. Antennas Propagat., Vol. AP-6, pp. 348-359, Oct. 1958.

[5] P.H. Pathak, "An aymptotic analysis of the scattering of plane waves by a smooth convex cylinder," Radio Sci., Vol. 14, pp. 419-435, 1979.

[6] J.B. Keller, "Diffraction by a convex cylinder," IEEE Trans. Antennas Propagat., Vol. AP-24, pp. 312-321, 1956.

[7] -----, "Geometrical theory of diffraction," J. Opt. Soc. Amer., Vol. 52, pp. 116-130, 1962.

[8] J.J. Bowman, T.B.A. Senior and P.L.E. Uslenghi, "Electromagnetic and Acoustic Scattering by Simple Shapes," Amsterdam: North-Holland, 1969.

[9] N.A. Logan and K.S. Yee, "Electromagnetic Waves," edited by R.E. Langer, University of Wisconson Press, Madison.

[10] R.G. Kouyoumjian and P.H. Pathak, "A uniform geometrical theory of diffraction for an edge in a perfectly conducting surface," Proc. IEEE, Vol. 62, pp. 1448-1461, 1974.

[11] N.A. Logan, "General Research in Diffraction Theory," Vol. 1, LMSD-288087, Missiles and Space Div., Lockheed Aircraft Corp., Sunnyvale, Calif.

[12] L.W. Pearson, "A scheme for automatic computation of Fock-type integrals," IEEE Trans. Antennas Propagat., Vol. AP-35, pp. 1111-1118, Oct. 1987.

[13] H. Kim and N. Wang, "UTD solution for electromagnetic scattering by a circular cylinder with thin lossy coatings," IEEE Trans. Antennas Propagat., Vol. AP-37, pp. 1463-1472, Nov. 1989.

[14] L. Felson and N. Marcuvitz, "Radiation and Scattering of Waves," Prentice Hall, 1973.

[15] B.K. Singaraju, D.V. Giri and C.E. Baum, "Further development in the application of contour integration to the evaluation of the zero of analytic functions and relevant computer programs," Math. Note 42, March 1976.

List of Figures

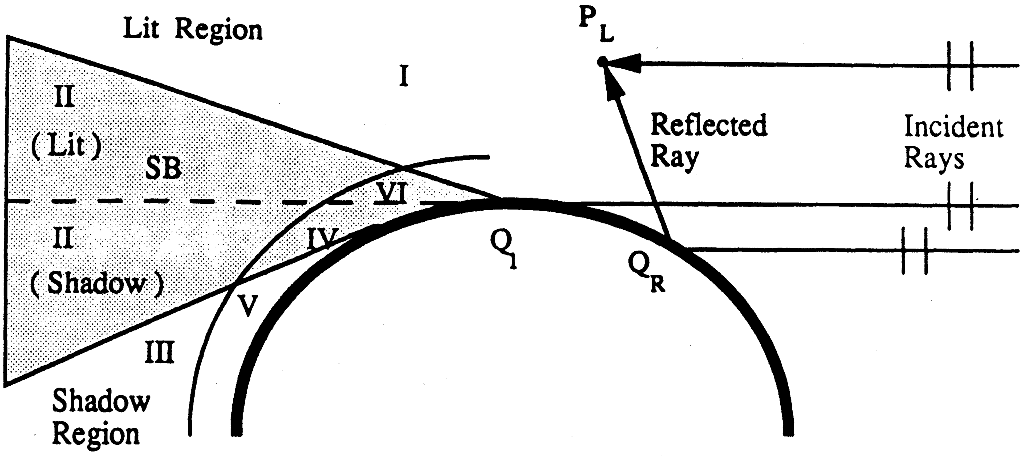

Fig. 1. Different regions associated with the plane wave scattering from a smooth convex cylinder.

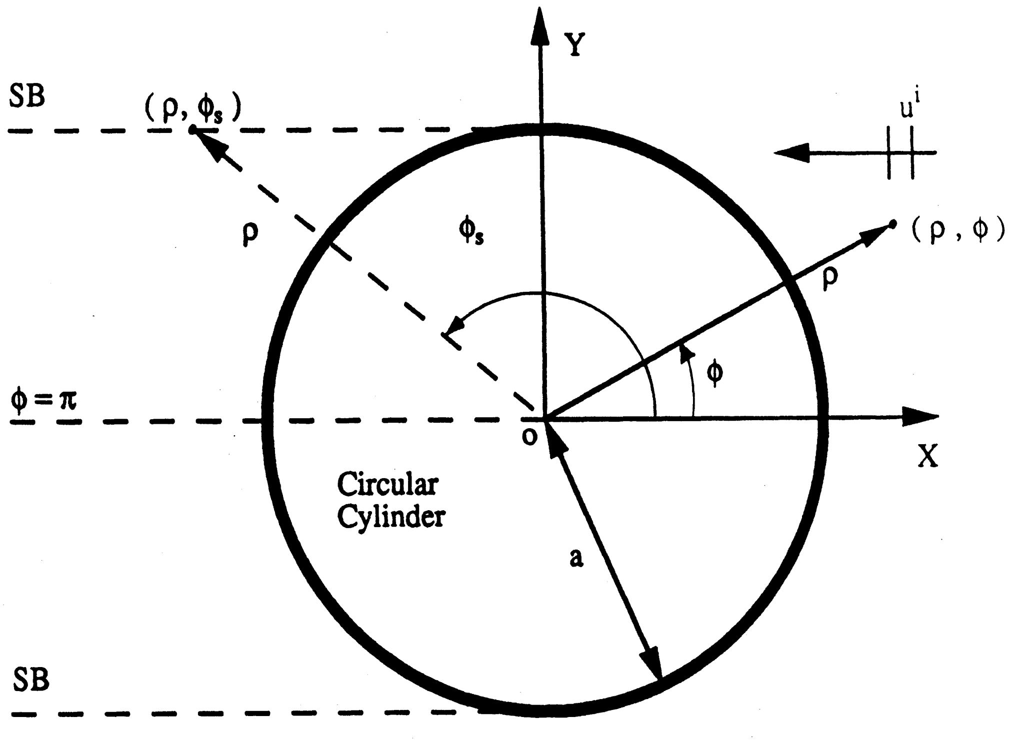

Fig. 2. Geometry of the canonical problem.

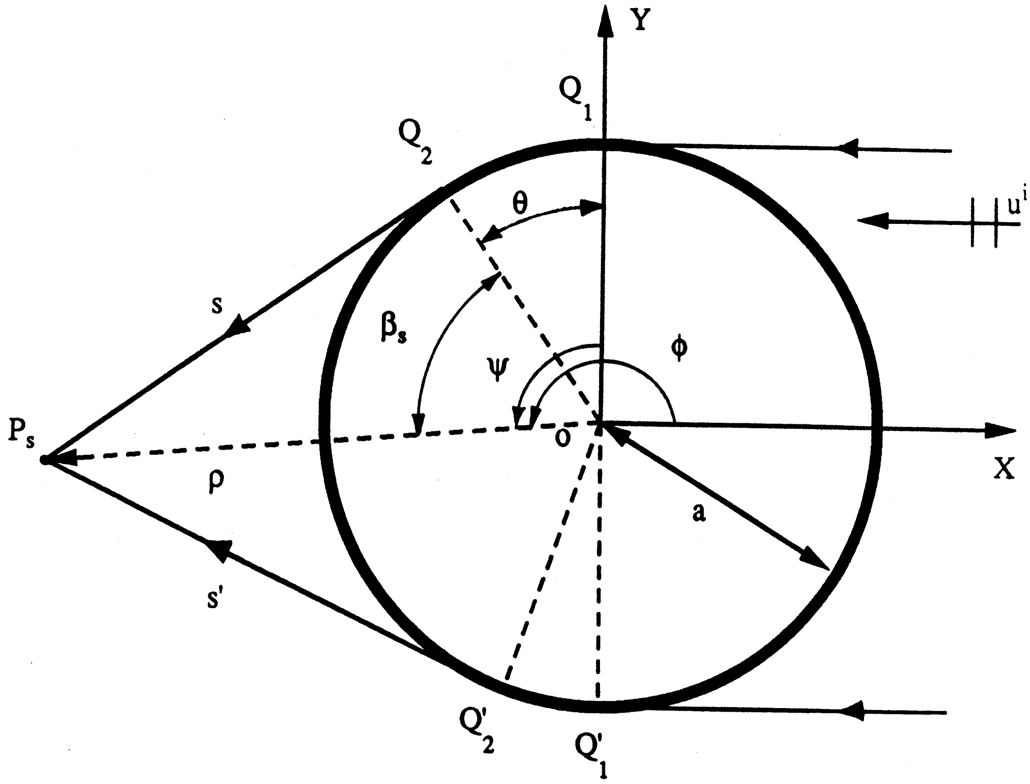

$$s^2 = \rho^2 - a^2$$

$$\beta_s = \cos^{-1}\frac{a}{\rho}$$

$$\theta = \psi - \beta_s$$

Fig. 3. Ray paths for the shadow region.

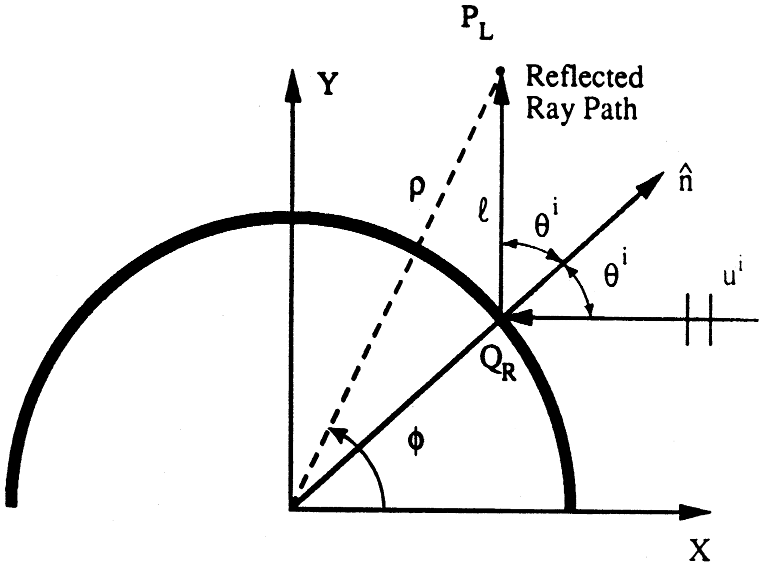

Fig. 4. Reflected ray path for the lit region.

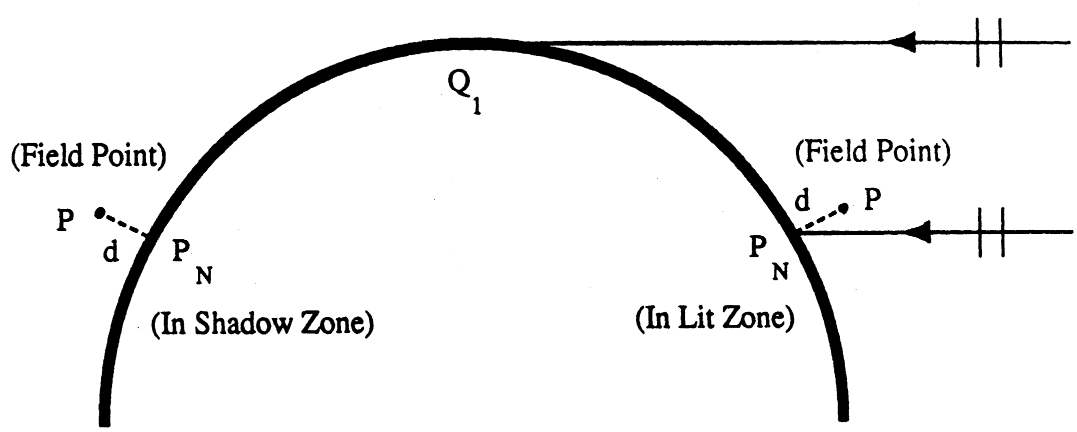

Fig. 5. The projection of the field point P in the direction of the surface normal at P_N .

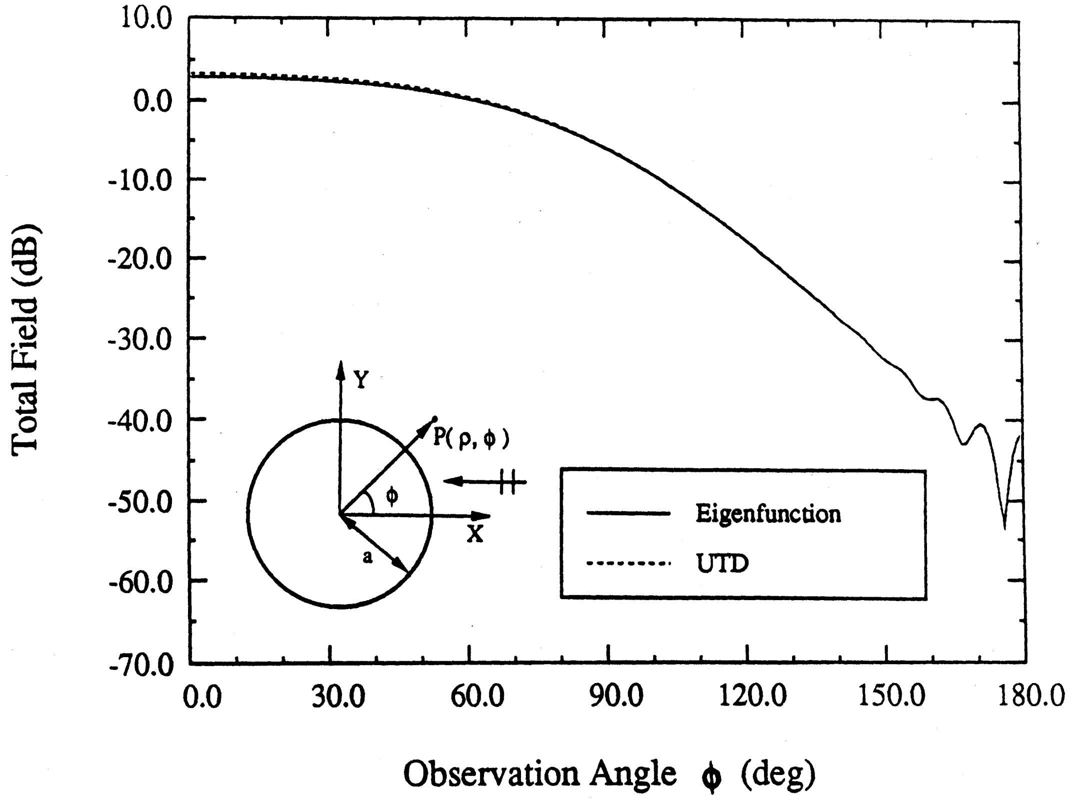

(a)

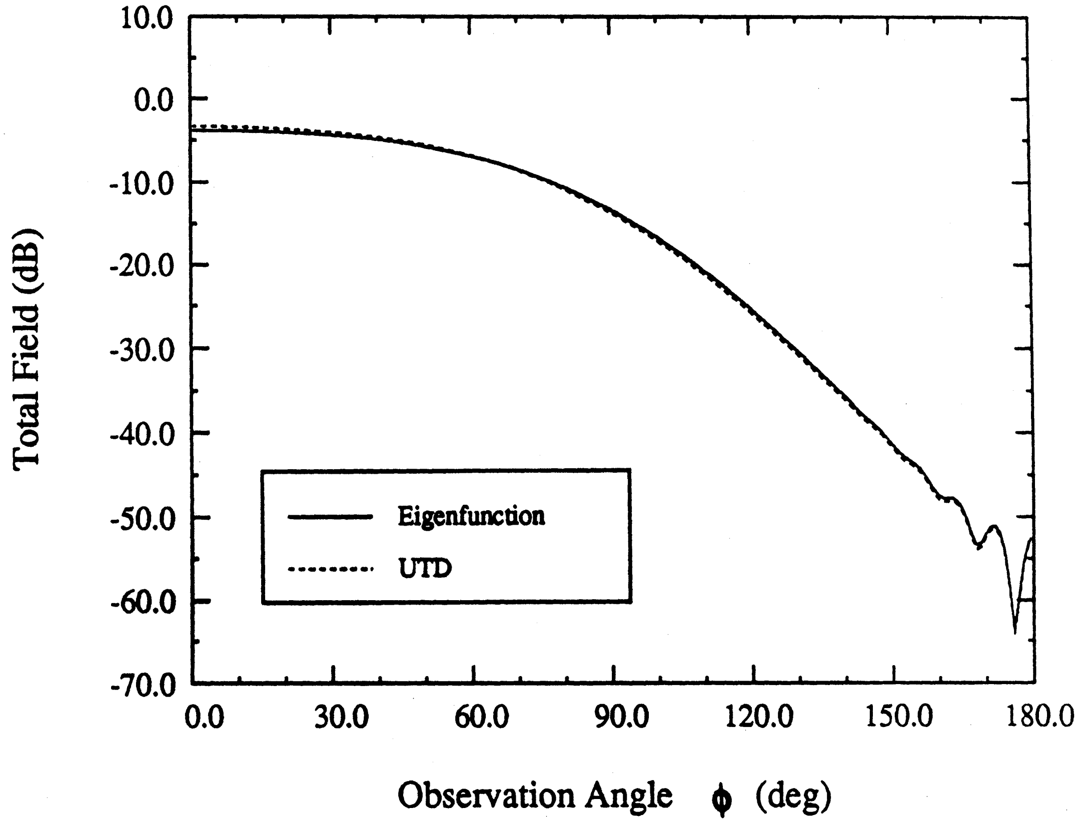

(b)

Fig. 6. Bistatic scattering pattern of a circular impedance cylinder with $a = 3\lambda$, $\rho = 3.05\lambda$ and $\eta = 1 + j\ 1$ (a) E - polarization (b) H-polarization.

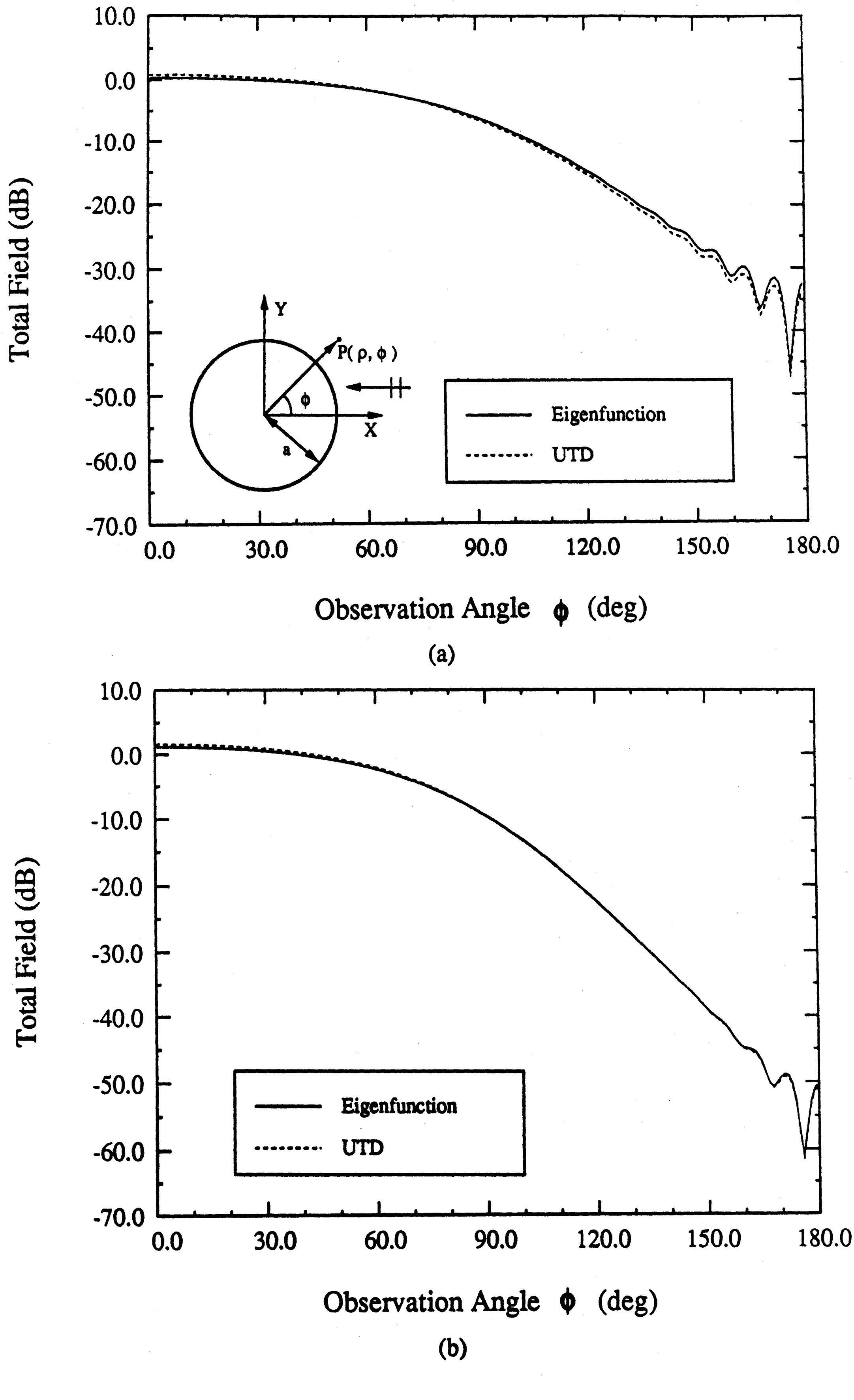

Fig. 7. Bistatic scattering pattern of a circular impedance cylinder with $a = 3\lambda$, $\rho = 3.05\lambda$ and $\eta = 1 - j\,1$ (a) E - polarization (b) H-polarization.

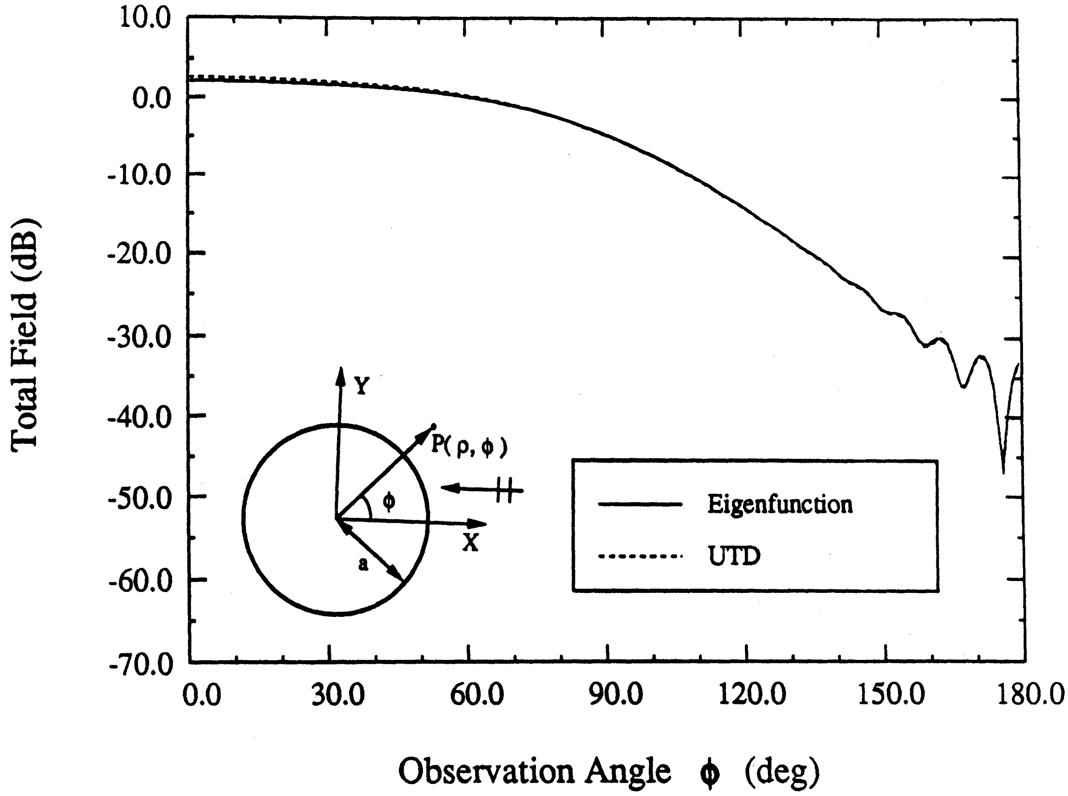

(a)

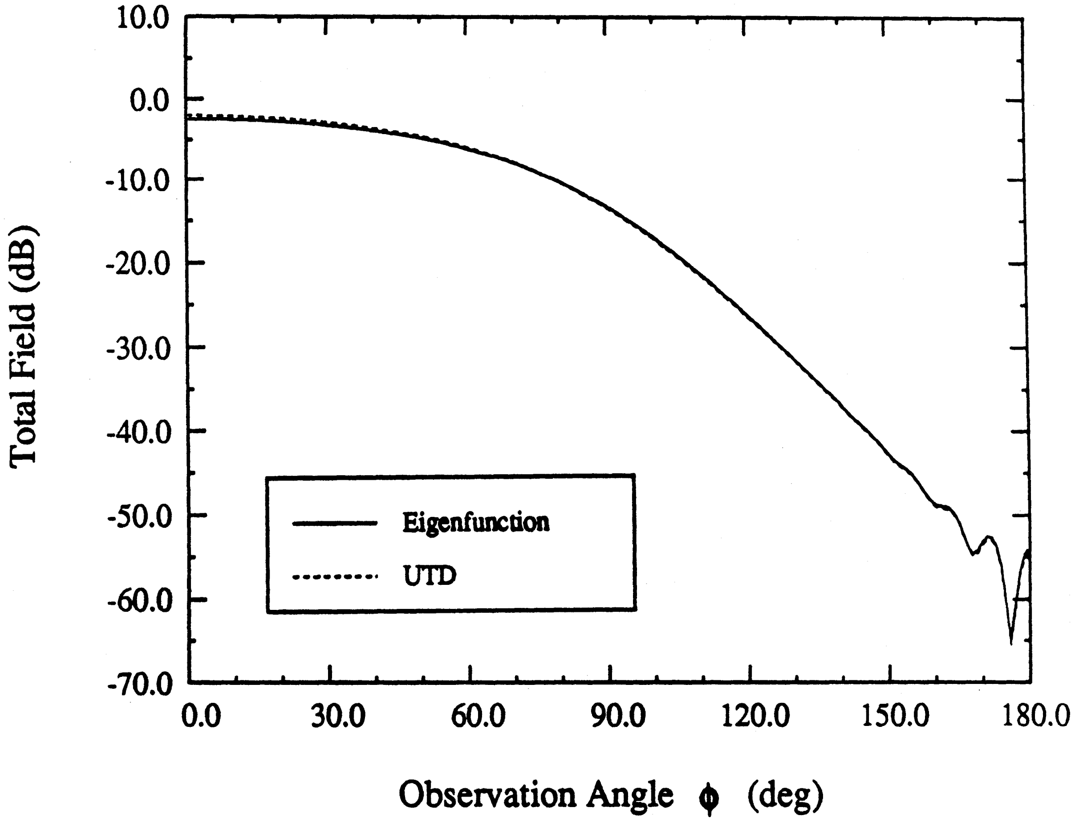

(b)

Fig. 8. Bistatic scattering pattern of a circular impedance cylinder with $a = 3\lambda$, $\rho = 3.05\lambda$ and $\eta = 2$ (a) E - polarization (b) H-polarization.

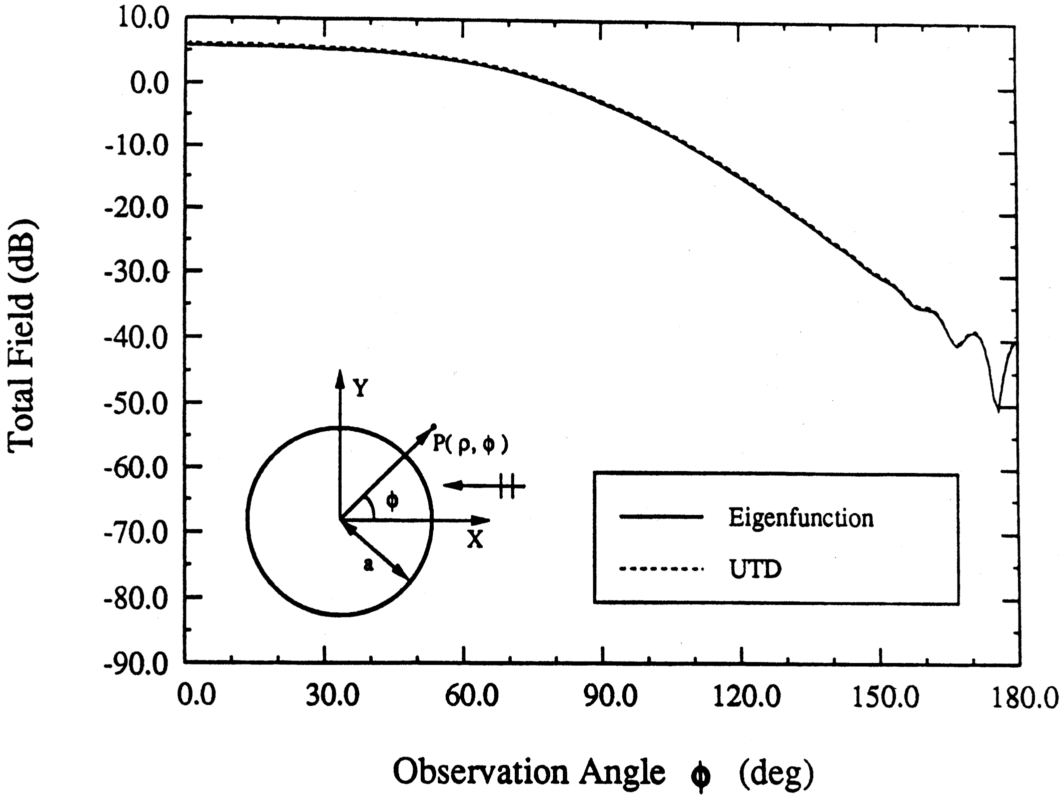

(a)

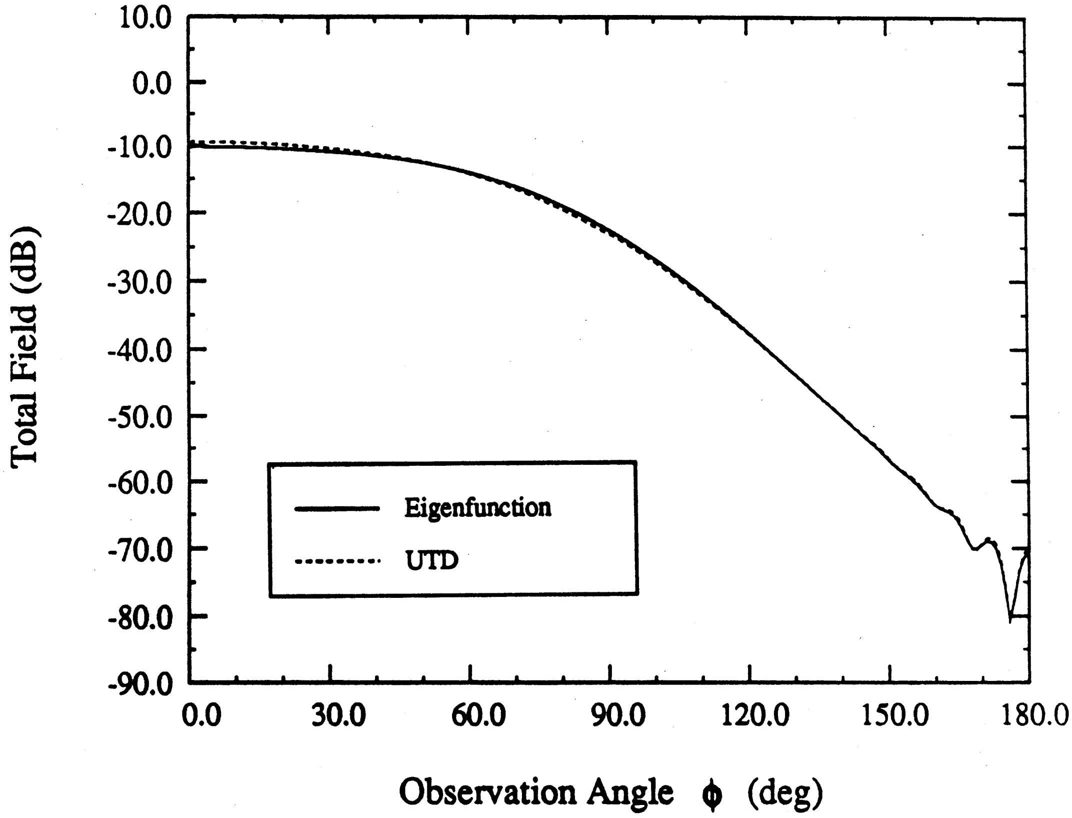

(b)

Fig. 9. Bistatic scattering pattern of a circular impedance cylinder with $a = 3\lambda$, $\rho = 3.05\lambda$ and $\eta = j\,2$ (a) E - polarization (b) H-polarization.

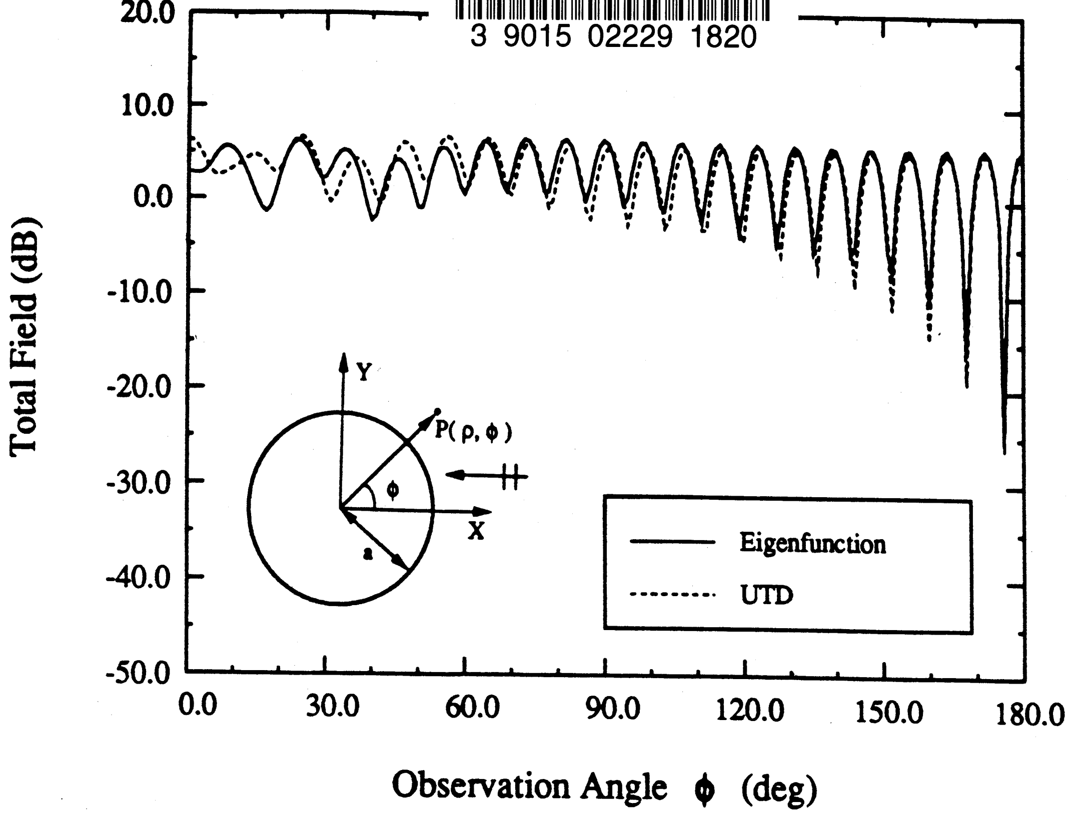

(a)

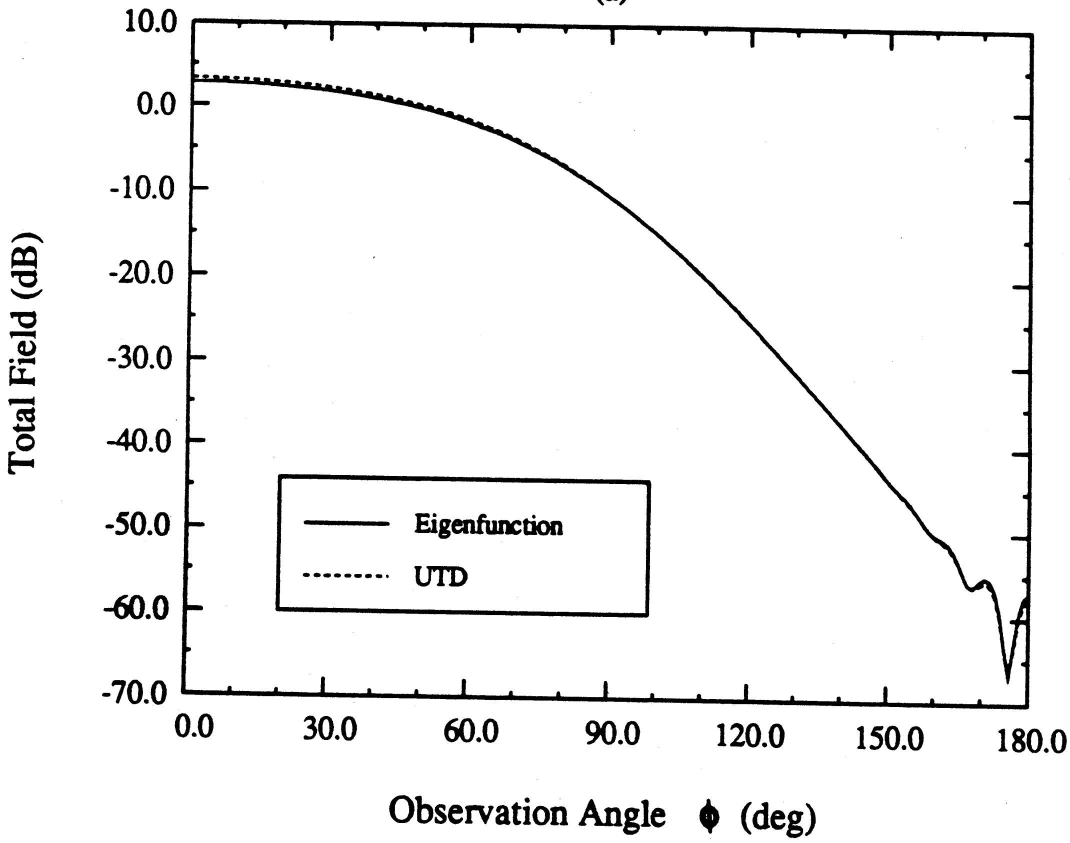

(b)

Fig. 10. Bistatic scattering pattern of a circular impedance cylinder with $a = 3\lambda$, $\rho = 3.05\lambda$ and $\eta = -j\,2$ (a) E-polarization (b) H-polarization.